Supporting Information

Protein Nanostructures Produce Self-Adjusting Hyperpolarized Magnetic Resonance Imaging Contrast through Physical Gas Partitioning

Martin Kunth[1,2], George J. Lu[1], Christopher Witte[2], Mikhail G. Shapiro[1], Leif Schröder[2].

[1]California Institute of Technology, Division of Chemistry and Chemical Engineering, Pasadena, California 91125, USA
[2]Leibniz-Forschungsinstitut für Molekulare Pharmakologie (FMP), 13125 Berlin, Germany

Table of Contents

1 Classic CEST Site Occupancy

For host-guest complex formation, the host occupancy β is given as a function of the binding constant, K_B, and the concentration of free atoms in pool A: $\beta = x/(x + 1)$ with $x = K_B[A]$.[1] Hence, the occupancy increases only marginally for typical hosts like CrA when the concentration of the bulk pool increases. Achieving $\beta \approx 90\%$ requires at least a 10-fold increase in [A].

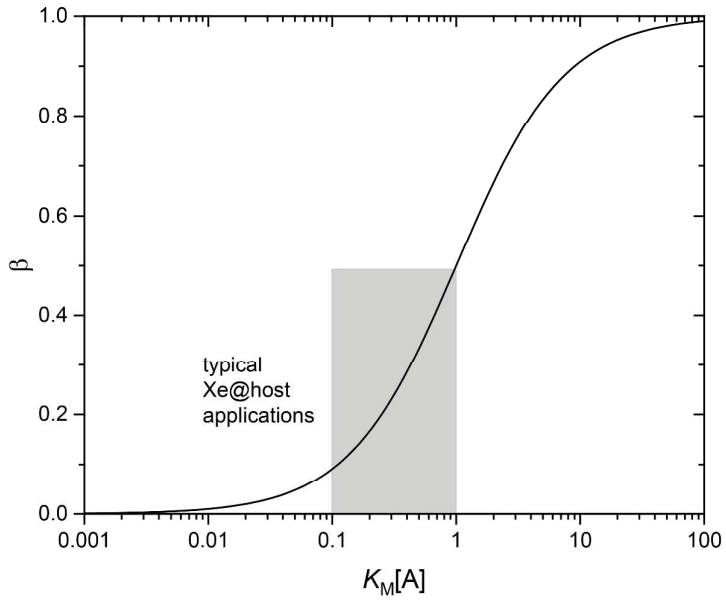

Figure S1. Plot of the occupancy β as a function of the product of binding constant and concentration of pool A. Xe-host systems typically yield values for $K_M[A] \approx 0.1 \ldots 1$.

2 Estimation of apparent T_2 Relaxation

The presence of GVs causes rapid exchange and thus a fast decay of transverse magnetization. In order to estimate the apparent T_2 time constant, we evaluated the FID decay after small flip angle excitation that is used for flip angle calibration after repetitive excitation as described in Ref. [2]. An exemplary signal decay is shown in Fig. S2 for Mega GVs (0.67 nM concentration in PBS, $T = 295$ K) and yields a value of $T_{2,app} = (2.2 \pm 0.5)$ ms.

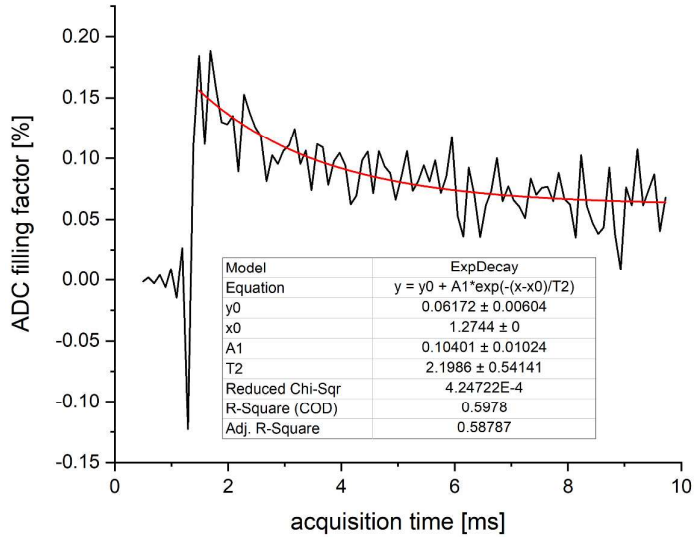

Figure S2. FID decay after small flip angle excitation of dissolved Xe in the presence of Mega GVs at 0.67 nM in PBS, T = 295 K.

3 Xenon Gas Pressure Dependence of *Mega* GVs and Cryptophane-A

Table S1 lists the xenon interaction parameters for GVs from *Mega* (data shown in Figure 4 in the main manuscript). Figure S3 shows the 1:1 xenon-Cryptophane-A interaction in chemical equilibrium in more detail (interaction parameters listed in Table S2). The experiment for CrA was done with identical parameters as in Figure 4 in the main manuscript, besides that the concentration was [CrA] = 5 µM and the RF cw saturation pulses were weakened to match the slower exchange rate of CrA of ca. 20 s^{-1}.

Table S1. Xenon-host interaction parameters obtained from qHyper-CEST for *Mega* GVs (180 pM) for different total pressures.

total pressure / bar	[Xe] / µM	relative chemical shift / ppm	bound xenon fraction	host capacity	exchange rate / (s^{-1})
4.5	974.4 ± 9.7	-164 ± 3	0. 00083 ± 0.00008	3,500 ± 60	23,500 ± 4,100
3.5	757.9 ± 7.6	-160 ± 1	0. 00096 ± 0.00004	3,010 ± 140	22,900 ± 1,300
2.5	541.3 ± 5.4	-160 ± 1	0. 00098 ± 0.00004	2,150 ± 100	23,600 ± 1,900
1.5	324.8 ± 3.2	-166 ± 3	0. 00100 ± 0.00007	1,370 ± 60	24,500 ± 3,500
1.2	259.8 ± 2.6	-157 ± 2	0.00081 ± 0.00005	890 ± 40	22,600 ± 2,800

Table S2. Xenon-host interaction parameters obtained from qHyper-CEST for Cryptophane-A (10 µM) for different total pressures.

total pressure / bar	[Xe] / µM	relative chemical shift / ppm	bound xenon fraction	host occupancy / %	exchange rate / (s^{-1})
4.5	974.4 ± 9.7	-132.89 ± 0.01	0.00578 ± 0.00064	56 ± 4	16 ± 3
3.5	757.9 ± 7.6	-132.83 ± 0.006	0.0073 ± 0.0086	55 ± 77	13 ± 20
2.5	541.3 ± 5.4	-132.82 ± 0.004	0.00713 ± 0.00226	39 ± 13	16 ± 10
1.5	324.8 ± 3.2	-132.78 ± 0.004	0.0096 ± 0.00318	31 ± 10	17 ± 13
1.2	259.8 ± 2.6	-132.78 ± 0.005	0.024 ± 0.046	62 ± 120	6 ± 7

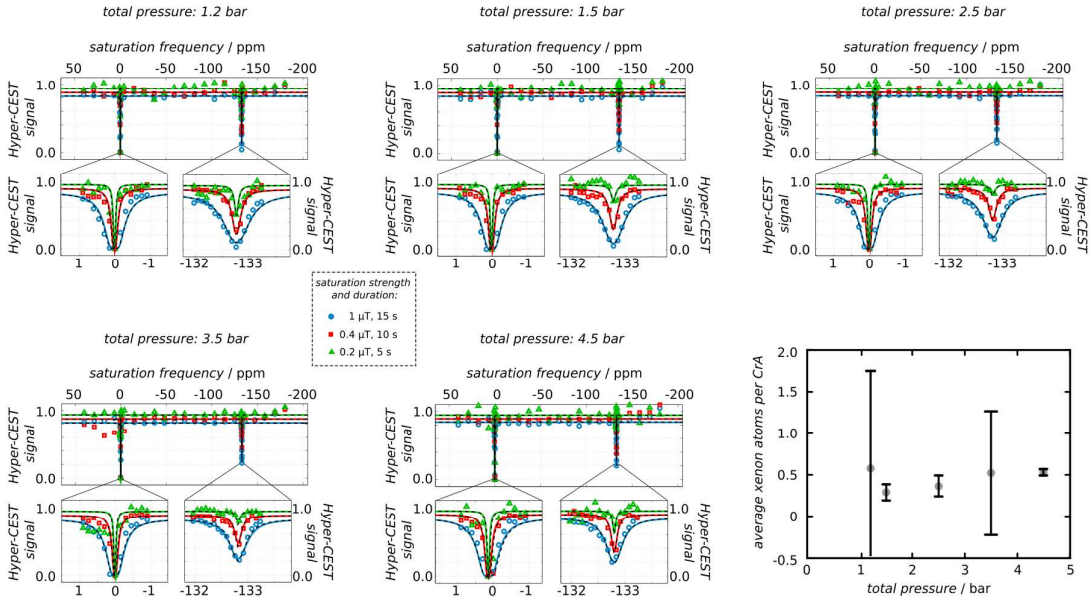

Figure S3. Xenon interaction with Cryptophane-A as a function of total pressure.

4 Gas Vesicle Stability Test for qHyper-CEST Measurements

Figures S4a-c show a total of four and five, respectively, consecutive recorded *z*-spectra from the same sample without replacing gas vesicles for *Mega* GVs (xenon gas total pressures of 1.2 bar and 1.8 bar) and gas vesicles from *Ana* (2.8 bar). Whereas the intensity of the Hyper-CEST effect for *Mega* reduced insignificantly after fourth repetition, *z*-spectra from *Ana* showed a minor change at the fifth repetition. In conclusion, we could record all three *z*-spectra for *Ana* and *Mega* with the same sample before moving to the next overpressure with a fresh sample of the same gas vesicle concentration. In contrast, we replaced *Halo* containing samples by fresh ones of the same concentration for every *z*-spectrum acquisition.

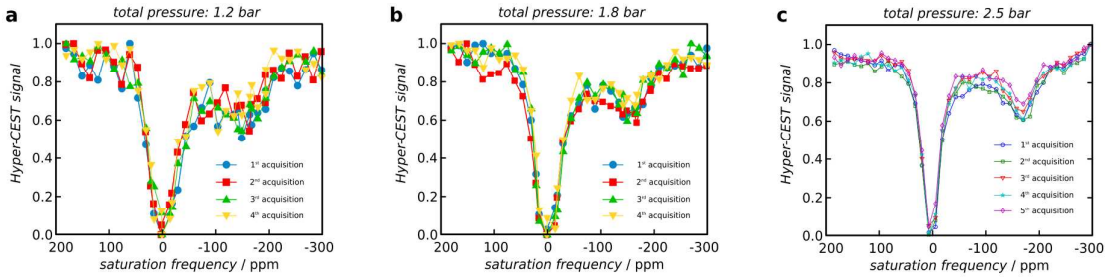

Figure S4. Stability test of gas vesicles from *Mega* ((a) 1.2 bar total pressure and (b) 1.8 bar) and *Ana* ((c) 2.5 bar total pressure).

5 Ideal Gas Law Considerations for Gas Vesicles

In the following, the xenon filling factor for each type of gas vesicle is compared to predictions according to the ideal gas law. Since all samples were measured at a temperature of 295 K, the volume of an ideal gas is given by

$$V_\mathrm{m} = \frac{N_\mathrm{A} \cdot k_\mathrm{B} \cdot T}{p} = \frac{(6.022 \cdot 10^{23}\,\mathrm{mol^{-1}}) \cdot (1.381 \cdot 10^{-23}\,\mathrm{J \cdot K^{-1}}) \cdot (295\ \mathrm{K})}{101.325\,\mathrm{kPa}} = 24.2125\ \mathrm{L/mol} \quad \text{(S1)}$$

at normal pressure p, using Avogadro's number N_A and Boltzmann's constant k_B. The mole fraction was calculated as

$$\text{mole fraction} = \frac{\text{on} - \text{average xenon atom capacity per gas vesicle}}{N_\mathrm{A}} \quad \text{(S2)}$$

The volume fraction in liter was calculated by

$$\text{volume fraction in liter} = \text{mole fraction} \cdot V_\mathrm{m} \quad \text{(S3)}$$

and the xenon filling factor yields to

$$\text{xenon filling factor} = \text{volume fraction in liter} \cdot V_\mathrm{GV} \quad \text{(S4)}$$

5.1 *Bacillus Megaterium* (*Mega*)

From gas vesicles derived from *Mega*, we measured an on-average xenon atom capacity per gas vesicle of 890 $\mathrm{bar^{-1}}$ (compare with Figure 4 in the main manuscript). The gas vesicle volume (determined from TEM data; see Table 1 in the main manuscript) was on average $6.5 \cdot 10^{-19}$ L (= 0.65 aL). With these values and Equations (S1-S4), we calculated the

mole fraction:	$1.47791 \cdot 10^{-21}$ mole/bar
volume fraction in liter:	$3.5784 \cdot 10^{-20}$ L/bar
xenon filling factor:	5.5 %

5.2 *Anabaena Flos-Aquae* (*Ana*)

From gas vesicles derived from *Ana*, we measured an on-average xenon atom capacity per gas vesicle of 6,610 bar^{-1} (Figure S5). The gas vesicle volume (determined from TEM data; see Table 1 in the main manuscript) was on average $6.05 \cdot 10^{-18}$ L. With these values and Equations (S1-S4), we calculated the

mole fraction:	$1.09764 \cdot 10^{-20}$ mole/bar
volume fraction in liter:	$2.65767 \cdot 10^{-19}$ L/bar
xenon filling factor:	4.4 %

5.3 *Halobacteria* (*Halo*)

From gas vesicles derived from *Halo*, we had only at most gentle bubbling success with quantitative experiments. We measured an on-average xenon atom capacity per gas vesicle of 5,800 at a total pressure of 1.2 bar (see Fig. 3c and Table 2 in the main manuscript). Thus, the on-average xenon atom capacity per bar is estimated by 5,800/(1.2 bar) = 4,833 bar^{-1}. The gas vesicle volume (determined from TEM data; see Table 1 in the main manuscript) was on average $6.25 \cdot 10^{-18}$ L. With these values and Equations (S1-S4), we calculated the

mole fraction:	$8.02557 \cdot 10^{-21}$ mole/bar
volume fraction in liter:	$1.94319 \cdot 10^{-19}$ L/bar
xenon filling factor:	3.1 %

The slightly smaller than 5 % xenon filling factor for gas vesicles from *Ana* originated from their higher fragility, compared to *Mega*, causing the initial slope in Figure S5 to be slightly underestimated. Similar consideration for the measurement with gas vesicles from *Halo* holds. In addition, *Halo* is known to be more fragile than *Ana* thus underestimating the gas capacity even more.

6 Elastic Scaling for Gas Vesicles Derived from *Ana*

The ideal gas behavior was also tested for gas vesicles from *Ana* (Figure S5), in a similar fashion as done for gas vesicles from *Mega* (shown in Figure 4 in the main manuscript). However, although *Ana* gas vesicle loss was observed for total pressures larger than 2.5 bar, the first two data points at most gentle overpressures could be used to extract an on-average number of xenon atoms per gas vesicle of (6,610 ± 150) bar^{-1}. This is ca 7.4-fold larger than the slope for *Mega*, whereas the volume of both GV types scales with a factor of 9.2 (6.05 aL vs. 0.65 aL). We thus assume that the integrity of *Ana* GVs was already partially compromised for the second pressure setting and the slope was slightly underestimated from these two data points.

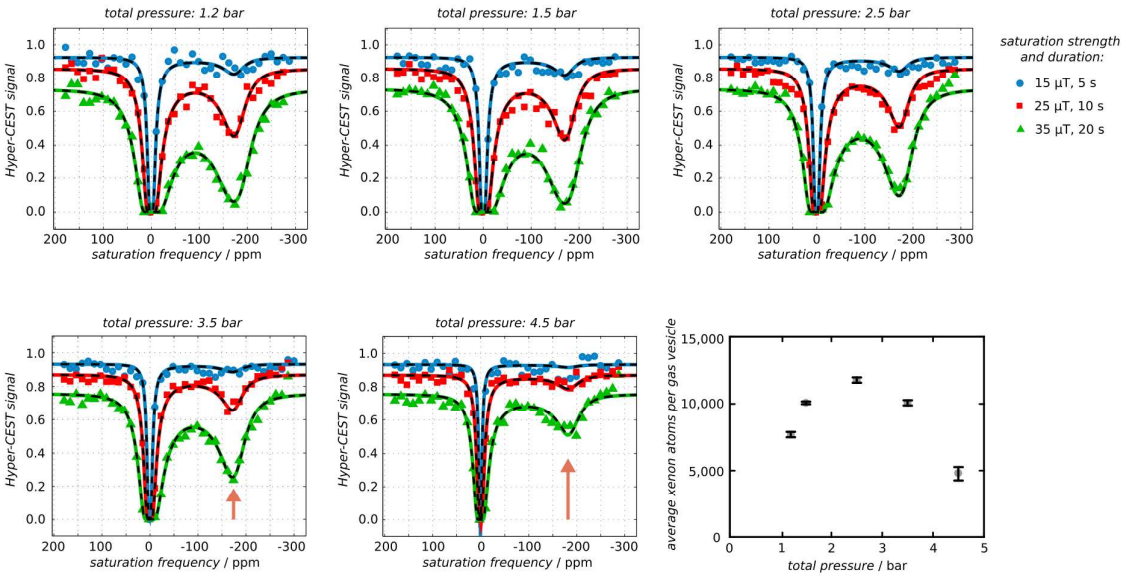

Figure S5. Elastic scaling for gas vesicles derived from *Ana*. For total pressures of 2.5 bar to 4.5 bar, the *Ana* gas vesicle concentration was no longer conserved during *z*-spectra acquisition and gas vesicles collapsed/ bursted which became evident by the loss of the intensity of the Hyper-CEST effect (red arrow). In regard to the on-average number of xenon atoms per gas vesicle, at higher total pressures the data no longer followed the linear relationship as observed for the much more stable gas vesicles from *Mega* (see Figure 4 in the main manuscript).

7 Classification of Contrast Build-Up

Host structures with high turnover rates (*e.g.*, fast xenon exchange and high xenon capacity) provide high CEST efficiency because they build-up the contrast fast. We classified the (hypothetical maximum) potential of each type of gas vesicles that were studied here by simulating the xenon depolarization rate as a function of the RF cw saturation pulse strength (Figure S6) as described Ref. [3]. This model excludes spillover effects with direct RF cw saturation of free xenon and was done by the following formula:[3]

$$\lambda_{\mathrm{depol}}(B_1, k_{\mathrm{BA}}) = f_{\mathrm{B}}\, k_{\mathrm{BA}} \frac{(\gamma\, B_1)^2}{(\gamma\, B_1)^2 + k_{\mathrm{BA}}^2} \tag{S5}$$

$$\Leftrightarrow \qquad \lambda_{\mathrm{depol}}(B_1, k_{\mathrm{BA}}) \cdot \frac{[\mathrm{Xe}]}{[\mathrm{host}]} = \beta \cdot k_{\mathrm{BA}} \underbrace{\frac{(\gamma\, B_1)^2}{(\gamma\, B_1)^2 + k_{\mathrm{BA}}^2}}_{=\,\alpha} \tag{S6}$$

where α is the labeling efficiency of the RF cw saturation pulse. Modeling results in Figure S6 show that in particular for specific absorption rate compatible weak RF cw saturation strengths of < 10 µT, a single gas vesicle nanostructure depolarizes xenon > 10^5 times faster than a single Cryptophane-A molecule or > 10^3 times faster than a single Cucurbit[6]uril molecule in aqueous solution.

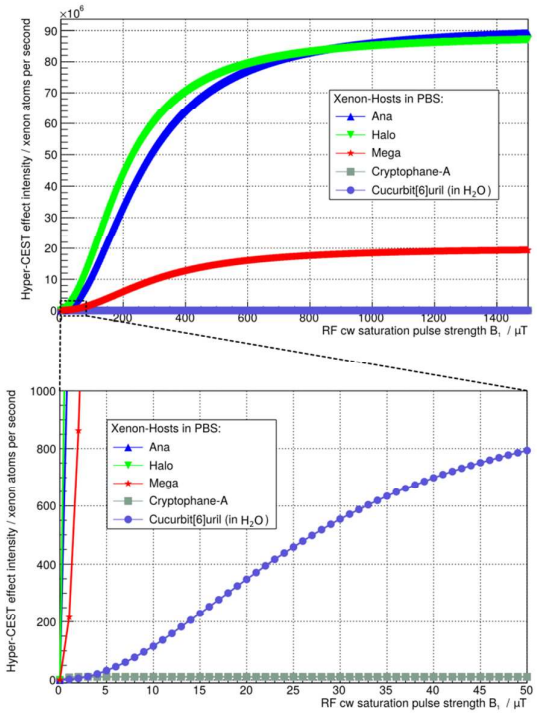

Figure S6. Comparison of contrast build up for gas vesicles derived from *Ana*, *Halo* and *Mega*; Cryptophane-A and Cucurbit[6]uril (in water)[3] were added for reference.

The hypothetical maximum effect as illustrated in Fig. S6 only becomes detectable if the saturation parameters are adjusted according to the exchange conditions. It is true that the GVs provide a favorable high gas turnover rate (product of exchange rate and occupancy), and this was also an argument for cucurbituril (CB6) over CrA. However, this does not necessarily fully translate into a scaling factor for the sensitivity. Fast exchange rates from larger structures like GVs have the potential to provide significantly improved sensitivity. Hardware and specific absorption rate limitations, however, might restrict the degree to which this potential can be used in real experiments. As known from ^{1}H CEST, optimum saturation transfer is achieved when the B_1 amplitude in Hz for cw saturation approximately matches the exchange rate out of the CEST pool. Our quantification yields k_{BA} = 19.3 kHz for Ana GVs and the ^{129}Xe Larmor frequency is 110.7 Hz/µT. Thus, the optimum B_1 to take full advantage of this fast exchange rate is ca. 1600 µT (Fig. S6), a value far beyond anything used for cw saturation.

To evaluate whether the kinetics of xenon exchange into GVs are diffusion-limited, we assume a steady state exchange of xenon between the bound and free pool (regardless of polarization). The experimentally measured exchange rate, representing the rate of xenon exit from the GV, is k_{BA}. The experimentally measured bound xenon fraction, f_B, represents the ratio $[Xe_{BOUND}] / [Xe_{FREE}]$. Under steady state $[Xe_{BOUND}]\ k_{BA} = [Xe_{FREE}]\ k_{AB}$, where the k_{AB} is the rate of xenon entry from solution into the GV compartment. Thus, $k_{AB} = f_B\ \ k_{BA}$. To estimate the mean diffusion of distance during the timescale $1/k_{AB}$, we use the 3-dimensinoal diffusion equation $d = (6 * 1/k_{AB} * D)^{1/2}$, where D is the diffusivity of xenon in water (1900 µm^2 s^{-1} at room temperature from NMR measurements[4]). This length scale can be compared to the expected mean separation between a suspension of GVs at

concentration [GV], which can be calculated as: ([GV] * N_A * 1000 L m^{-3})$^{1/3}$, where N_A is Avogadro's number.

8 Workflow of Data Quantification

All *z*-spectra were derived automatically from two region-of-interests within the signal and noise areas of the MR images (Figure S7) using C++ (version 4.9.2 on Debian 4.9.2-10) and Root[5] (version 6.10/06) with custom-designed scripts. *z*-Spectra fitting was done in Matlab 7 (The Mathworks, Natick, MA, USA) as described in Ref. [1].

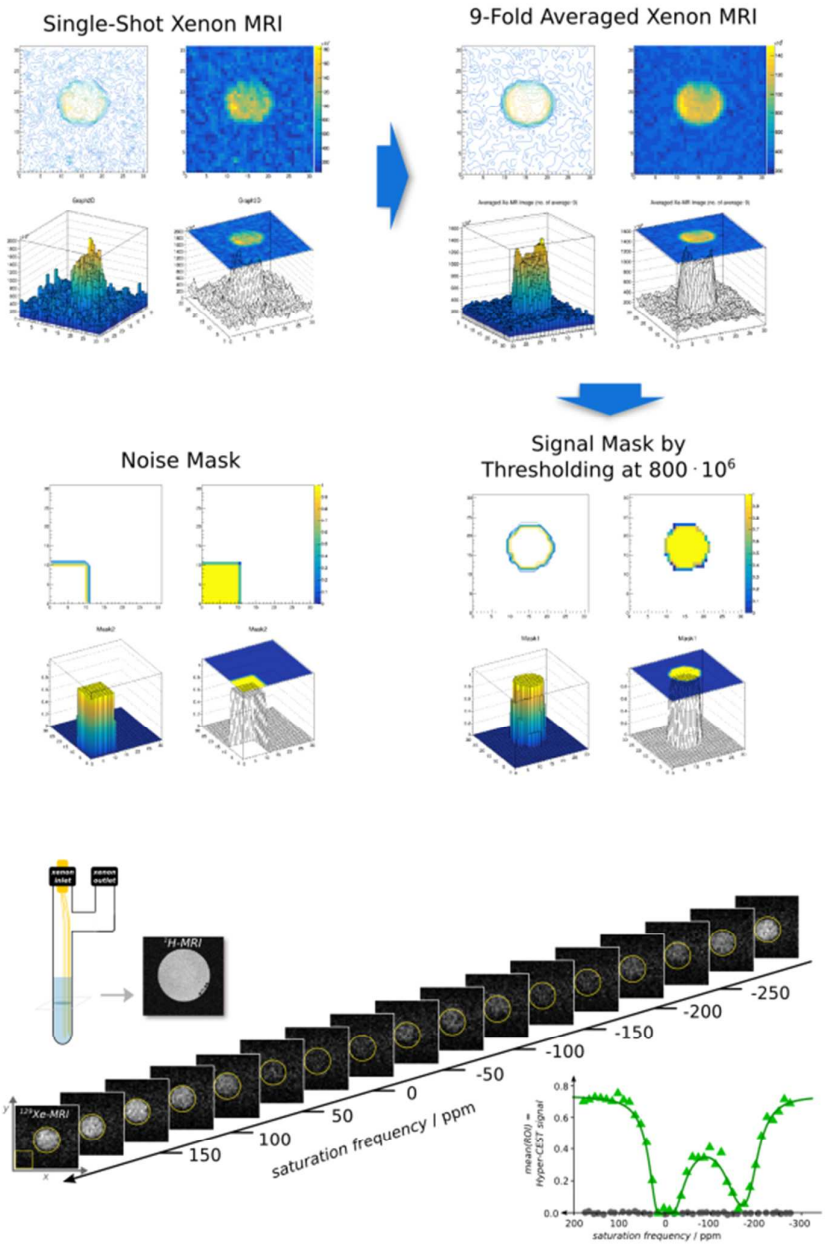

Figure S7. Automated *z*-spectrum determination by region-of-interest determination automation. The region-of-interest of the signal was obtained by thresholding 9-fold averaged Xe MR image (which is obtained from several images with signal from the *z*-spectrum for free). The noise region-of-interest was set to a 10 × 10 matrix constantly to the bottom left of the image matrix. The gas vesicle containing bubbling phantom (including proton-MRI of its cross-section) is shown on the bottom left.

9 Xenon Gas Pressure Dependence in *z*-Spectra

Figures S8 and S9 show the *z*-spectra for gas vesicles derived from *Mega* and Cryptophane-A, respectively, for xenon gas total pressures of {1.2, 1.5, 2.5, 3.5, 4.5} bar. The error bars indicate the standard deviation of the signal within each region-of-interest (see Figure S7).

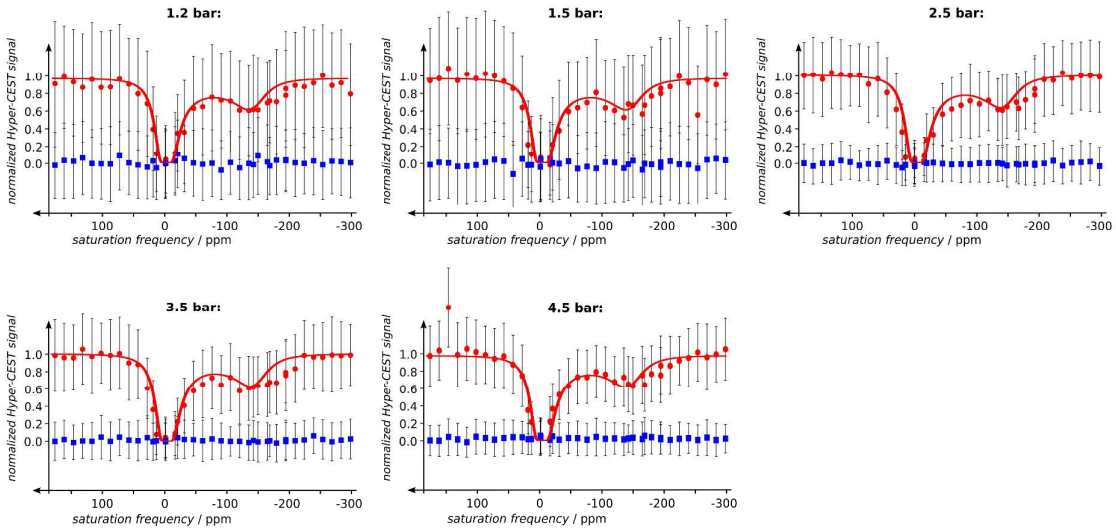

Figure S8. *z*-Spectra for gas vesicles derived from *Mega* at different total pressures (obtained from MR images using the automated framework shown in Figure S7; RF cw saturation: 15 µT for 10 s; gas vesicle concentration: ca. 180 pM in dPBS).

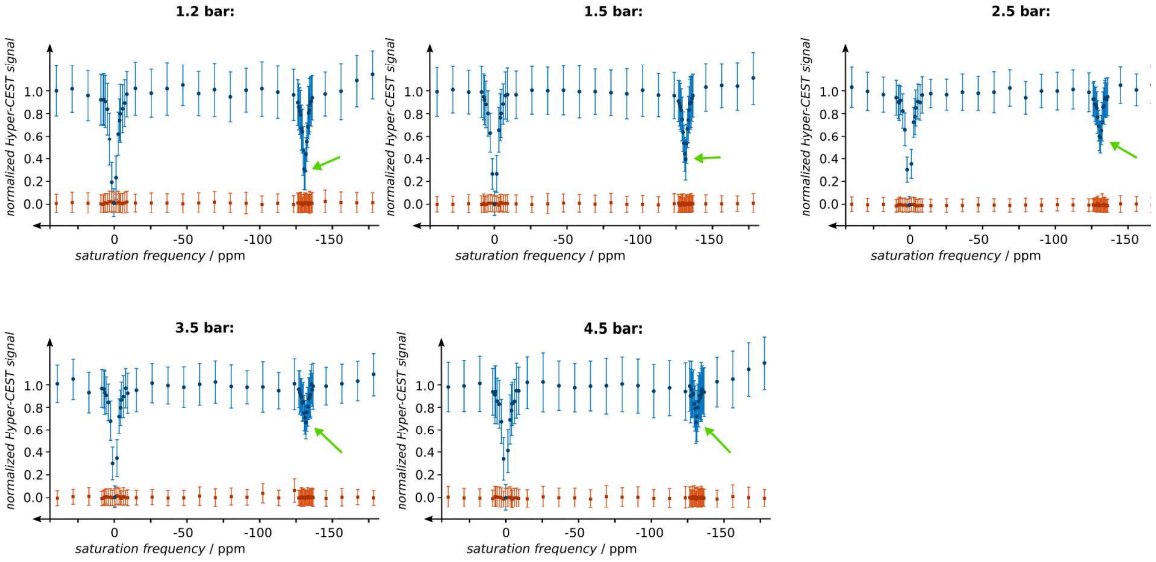

Figure S9. Cryptophane-A *z*-spectra at different total pressures (5 µM in dPBS; RF cw saturation: 15 µT for 10 s) obtained from MR images using the automated framework shown in Figure S7. The green arrow indicates change in intensity of Hyper-CEST effect of the Cryptophane-A-bound xenon resonance.

10 References

(1) Kunth, M.; Witte, C.; Schröder, L. Quantitative Chemical Exchange Saturation Transfer with Hyperpolarized Nuclei (QHyper-CEST): Sensing Xenon-Host Exchange Dynamics and Binding Affinities by NMR. *J. Chem. Phys.* **2014**, *141*, 194202.

(2) L Lakshmanan, A.; Lu, G. J.; Farhadi, A.; Nety, S. P.; Kunth, M.; Lee-Gosselin, A.; Maresca, D.; Bourdeau, R. W.; Yin, M.; Yan, J.; Witte, C.; Foster, F. C.; Schröder, L.; Shapiro, M. Preparation of Biogenic Gas Vesicle Nanostructures for Use as Contrast Agents for Ultrasound and MRI. *Nature Protocols* **2017**, *12*, 2050–2080.

(3) Kunth, M.; Witte, C.; Hennig, A.; Schröder, L. Identification, Classification, and Signal Amplification Capabilities of High-Turnover Gas Binding Hosts in Ultra-Sensitive NMR. *Chem. Sci.* **2015**, *6*, 6069–6075.

(4) Weingärtner, H.; Haselmeier, R.; Holz, M. 129Xe NMR as a New Tool for Studying Gas Diffusion in Liquids: Self-Diffusion of Xenon in Water. *Chemical Physics Letters* **1992**, *195*, 596–601.

(5) Brun, R.; Rademakers, F. ROOT — An Object Oriented Data Analysis Framework. *Nuclear Instruments and Methods in Physics Research Section A: Accelerators, Spectrometers, Detectors and Associated Equipment* **1997**, *389*, 81–86.